SCIENTIFIC REPORTS
nature research

OPEN

Highly Responsive Ultraviolet Sensor Based on ZnS Quantum Dot Solid with Enhanced Photocurrent

Sellan Premkumar[1,3,4*], Devaraj Nataraj[1,2*], Ganapathi Bharathi[1], Subramaniam Ramya[1] & T. Daniel Thangadurai[5]

Detection of visible blind UV radiation is not only interesting but also of technologically important. Herein, we demonstrate the efficient detection of UV radiation by using cluster like ZnS quantum dot solid nanostructures prepared by simple reflux condensation technique. The short-chain ligand 3-mercaptopropionic acid (MPA) involved in the synthesis lead to the cluster like formation of ZnS quantum dots into solids upon prolonged synthesis conditions. The ZnS QD solid formation resulted in the strong delocalization of electronic wave function between the neighboring quantum dots. It increases the photocurrent value, which can be further confirmed by the decrease in the average lifetime values from 64 to 4.6 ns upon ZnS cluster like QD solid formation from ZnS QDs. The ZnS quantum dot solid based UV sensor shows good photocurrent response and a maximum responsivity of 0.31 (A/W) at a wavelength of 390 nm, is not only competitive when compared with previous reports but also better than ZnS and metal oxide-based photodetectors. The device exhibits a high current value under low-intensity UV light source and an on/off ratio of $I_{UV}/I_{dark} = 413$ at zero biasing voltage with a fast response. Further, photocurrent device has been constructed using ZnS quantum dot solid nanostructures with graphene hybrids as an active layer to improve the enhancement of photoresponsivity.

UV-photodetectors received great scientific attention owing to their significant commercial applications including water treatment, defense safety[1], flame detection, and space communication[2–5]. The commercially used silicon-based photodetector faces a major problem of low photon absorption capability in the Ultraviolet (UV) region due to its high reflection co-efficient[6]. Recently, numerous technological innovations have been reported in the detection of UV radiation, where several wide bandgap semiconducting materials were used for the photoactive materials in UV-photodetectors namely, SiC[6,7], ZnS[8], GaN[9–11], ZnO[12–14], Ga_2O_3[7,15,16] and Graphene QDs[17–19]. UV Photodetector constructed by using Metal oxide semiconductor as an active material delivers poor device performance due to its surface defects[20,21], which causes the slow recovery of photocurrent. Metal chalcogenides (S, Se, Te)[5,22–24] based photodetectors were considered to be the best alternative to metal oxide based photodetectors. The photoconductive type[8] and photodiode type technologies were mainly used in current research and commercial products of the UV photo-sensing field. Having a wide band gap semiconductor is a potential considerate for constructing UV photodetectors. There are several reports on the investigation of ZnS nanostructure based UV photodetectors[25–27]. For example; Yeonhokim *et al.*[28] demonstrated 1D ZnS nanobelt with graphene structure producing the responsivity of 1.2 mW/cm^2 power when illuminated at 300 nm UV light, where it delivered the photocurrent value of 0.115 mA[29]. Fang *et al.*, has reported ZnS nanobelts based photodetectors with the photocurrent value of 0.5 pA resulting in the low responsivity of 0.1 A/W[23]. An Qinwei et al also reported ZnS nanotube with silver nanowire-based UV photodetector[27]. However, these reported photodetectors displayed relatively low responsivity and slow photoresponse, caused by low carrier mobility. The three-dimensionally confined ZnS quantum dot system has been investigated over other nanostructures, because of its superior quality:

[1]Quantum Materials and Devices Laboratory, Department of Physics, Bharathiar University, Coimbatore, Tamil Nadu, 641046, India. [2]UGC-CPEPA Centre for Advanced Studies in Physics for the development of Solar Energy Materials and Devices, Department of Physics, Bharathiar University, Coimbatore, Tamil Nadu, 641046, India. [3]School of Chemistry and Chemical Engineering, Tianjin Polytechnic University, Tianjin, 300387, China. [4]Tianjin Key Laboratory of Green Chemistry and Process Engineering, and School of Material Science and Engineering, Tianjin Polytechnic University, Tianjin, 300387, China. [5]Department of Nanoscience and Technology, Sri Ramakrishna Engineering College, Coimbatore, Tamil Nadu, 641022, India. *email: sivajiisro@gmail.com; de.natraj2011@gmail.com

higher surface to volume ratio. But it has some difficulties in the electron transfer process between the quantum dots. The colloidal quantum dots are able to generate the electron-hole (e-h) pairs effectively; however all the photogenerated charges could not be transfered to the respesective electrodes to yield the best device performance. The photogenerated charges have to travel through the adjacent quantum dots, where they get trapped before reaching the electrodes. In addition, the large capping molecules will offer resistance to the transfer of charges between quantum dots.

In recent years a number of innovative research work were undergoing in the construction of ZnS nanostructure[29–31] based UV-photodetector with different morphologies like ZnS nanobelts[8,23,28,31,32], ZnS nanotubes[27] and ZnS nanowires[33,34], as an active layer. These type of one-dimensional[35] nanostructure-based UV photodetectors show relatively low responsivity and slow photoresponse due to low carrier mobility and high surface reactivity. ZnS Quantum dot has poor charge transport issue; as discussed before, in QDs system ligands molecules negative influence on the charge transport properties[36–38]. One possible way to address this problem is bringing the QDs closer enough by means of using short-chain ligands over the widely used lengthier ones (such as TOPO, TOP, Oleic acid, Oleylamine)[37,39,40]. Interconnecting the quantum dots with the help of short-chain ligands should enhance the performance of the device owing to its excellent inter-dot charge transport[41–44]. Such type of nanostructures is normally denoted as Quantum dot solids as it mimics the character of atomic solids. Like the arrangement of individual atoms can lead to the formation of atomic solids, quantum dot solid can be formed by means of an effective arrangement of quantum dots. In our previous work, we have attained CdTe QDs solid wire-like structure in the prolonged reaction condition, which shows better photocurrent response than quantum dots based device[43]. The bulk bandgap of CdTe lying in the visible region makes it more suitable for solar cell applications than acting as an UV sensing device. ZnS nanostructures have the bulk bandgap in the UV region making it a perfect choice as an active layer for UV photo-sensing device. With this basic knowledge, we have tuned the morphology of ZnS quantum dots to cluster like ZnS QDs solids by simply prolonging the reaction time. UV photodetector constructed using clusters like ZnS QDs solid exhibited better device performance over ZnS quantum dot based device due to the effective overlapping of electronic wavefunctions of neighboring quantum dots in the cluster state. To the best of our knowledge, these kinds of an interesting cluster like ZnS quantum-dot based photodetector device is not yet constructed till now. For attaining the improved charge carrier extraction and responsivity further, the ZnS quantum dot cluster like nanostructures were hybridized with graphene and used as an active layer for photodetector device[45,46]. The present paper discusses the methodology used for attaining clusters like nanostructures and their characterization, then finally the photocurrent study under UV light illumination.

Results and Discussion

Cluster like ZnS quantum dot solid formation. Figure 1(a,b) shows the UV-Vis absorption and PL emission spectra of ZnS samples prepared at different reaction time intervals. The optical UV absorption edge of the ZnS 6 hrs sample is observed around at 310 nm with a significant blue shift compared to the bulk ZnS band gap value of 340 nm[47] owing to the quantum confinement effect. To know about the emission behavior of these samples, we have recorded photoluminescence emission spectra by exciting the samples at their respective absorption maximum. Upon excitation at 310 nm the ZnS quantum dot exhibit emission around 445 nm which is shown in Fig. 1(b). The transition of electrons from a shallow state near the conduction band to the sulfur vacancies present near the valence band is the major reason for the emission observed at 445 nm (Fig. S1)[48]. Upon increasing the reaction time from 6 hrs we have noticed the improvement in the intensity of emission peak up to 24 hrs. Once when the reaction time crosses 24 hrs, the emission peak intensity gets decreased. This observation indicates the possibility of changes in the morphology of the samples, which were subjected to the prolonged synthesis duration. In order to quantify the morphological change, the samples are subjected to HR-TEM analysis with respect to the reaction time.

Figure 2(a–d) shows the HR-TEM results of ZnS quantum dot samples prepared at different reaction time duration such as 12 hrs and 24 hrs. Having a closer look at the HR-TEM images as shown in Fig. 2(a,b), one can see that there was no increase in the size of ZnS QDs beyond 5 nm; instead the ZnS QDs starts to agglomerate and form clusters with an increase of reaction time after 24 hrs. It means that the ZnS QD joins together to form a quantum dot cluster like solid structure. In this cluster state, the electronic wavefunctions of neighboring quantum dot get overlapped which leads to better carrier transport because of the delocalization effect. Due to this delocalization effect, we have attained quenching in emission starting from 24 hrs. The final hour reaction sample exhibits large clusters that contain interconnected ZnS quantum dots as shown in Fig. S2(a,b). The 48 hr prepared samples in the HRTEM images shows large size quantum dots clusters formed by the joining of individual quantum dots during prolonged time synthesis. We have subjected the as-prepared ZnS samples to TCSPC analysis by using a 390 nm pulsed excitation source. The PL decay lifetime curve is fitted with bi-exponential. It shows that the decay time of ZnS QDs decreased gradually with increasing reaction time intervals from 12 to 48 hrs as shown in Fig. 3. The calculated lifetime values presented in the Table 1, represents the decreases in the average lifetime values from 64 to 4.6 ns upon ZnS cluster like QD solid formation from ZnS QDs. It has to be noted that the faster component life time (τ_1) has an increased contribution to the overall lifetime value from 46% to 90%. From the above observation, we concluded that the cluster like ZnS quantum dot solid formation has resulted in the delocalization of excited charge carriers into nearby ZnS QDs, in the cluster like quantum dot solid structure, which decreases the PL emission intensity and corresponding reductions in the average lifetime. We believe that these interesting results could be effectively utilized to harvest the photoelectrons with enhanced performance in the photodetector application. Precisely, when the excitons are delocalized in a coupled QD solid system, their exciton binding energy decreases. This expected decrease in the binding energy charge carrier will make them available for relatively longer time at the excited states of the coupled system, and can be collected easily using appropriate electrodes. By collecting these delocalized excitons, the resultant photocurrent can be improved. The reported inorganic semiconductor-based UV photodetectors still have low electrical performance (charge

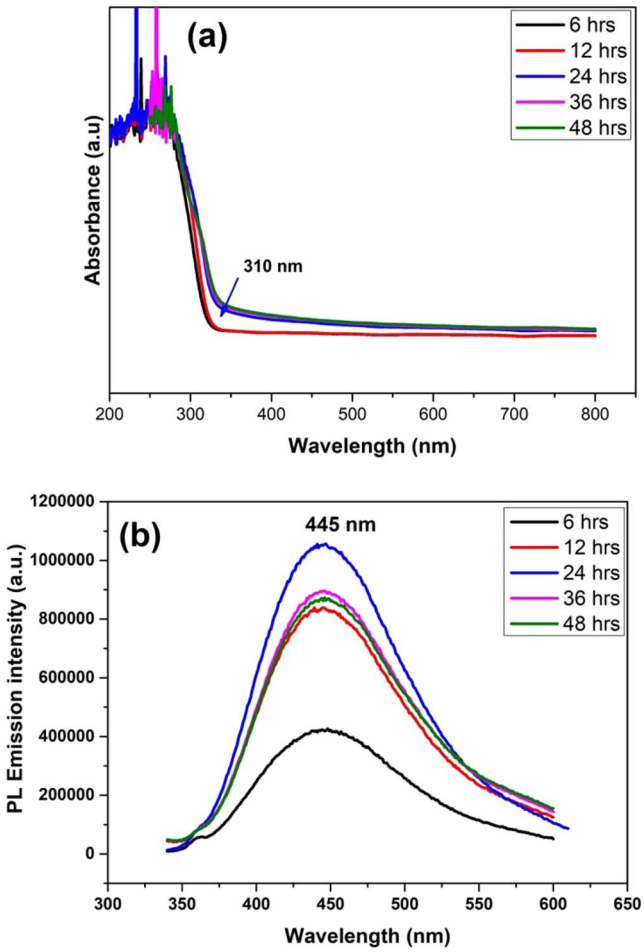

Figure 1. (**a**) UV-vis Absorbance spectra, and (**b**) Photoluminescence emission spectra of ZnS QDs samples prepared at different reaction time intervals (6, 12, 24,36, and 48 hrs).

transport properties). To overcome this limitation, the widely used option is hybridization with graphene, a better alternative to increase the photocurrent efficiency and the overall device performances. Herein, the graphene hybridization protocol is also utilized to extract the photoexcited electrons from the ZnS QDs nanostructure.

Investigation of graphene/ZnS quantum dot hybrids structure. From the literature reports, graphene has been widely used as the electron extractor or charge carrier collector to improve the efficiency of the optoelectronic devices[49–51]. In particular, the use of graphene to prepare efficient hybrid nanostructures in the field of solar cells and photodetectors has gained remarkable attention in recent years[17,29,51]. The reported hybrid nanostructures include Silicon/Graphene[6], ZnS/graphene[28,29], CdSe/graphene[52], CdTe/graphene[53,54], and ZnSe/ZnS:Graphene[30]. The responsivity of the photodetectors can be improved by effectively harvesting the excited charge carriers, irrespective of the illumination energy, i.e., the photoexcited charge carriers must be harvested from the photosensitizers before the recombination takes place. As discussed before, one possible way to achieve this is to harvest the excited charge carriers, immediately after the photoexcitation[55,56]. In the present case, we have introduced graphene in such a way that, it can be able to collect the photoexcited electrons from ZnS QDs, which in turn would enhance the photocurrent response of the photocurrent device. The graphene/ZnS quantum dot hybrids were synthesized by a modified protocol as described in the experimental section. Similar to the previous synthesis procedure, the samples were generated at different time intervals and then subjected to UV-vis absorption, PL emission and HRTEM analysis to investigate its morphological and optical properties. Figure 4(a,b) shows the optical UV absorption and PL emission spectra respectively, recorded for ZnS QD/graphene hybrids samples. In the case of 6 hrs sample, the blue-shifted absorption peak is observed at 285 nm compared to that of pure ZnS QDs sample, which confirms the formation of hybrid structures. The PL emission quenching was observed in the hybrid samples and weak blue-shifted emission at around 421 nm, compared to the bare ZnS samples (presented in Fig. 4(b)), which is recognized due to the transfer of photoexcited electrons from ZnS QDs to graphene system[57,58]. Further increasing the reaction time, increases the PL emission intensity up to 36 hrs, after which it remained the same. Figure 5(a,b) shows the monodispersed spherical shaped ZnS QDs particle decorated on the graphene layer (24 hrs) with an average particle size of about 8 nm, and the measured

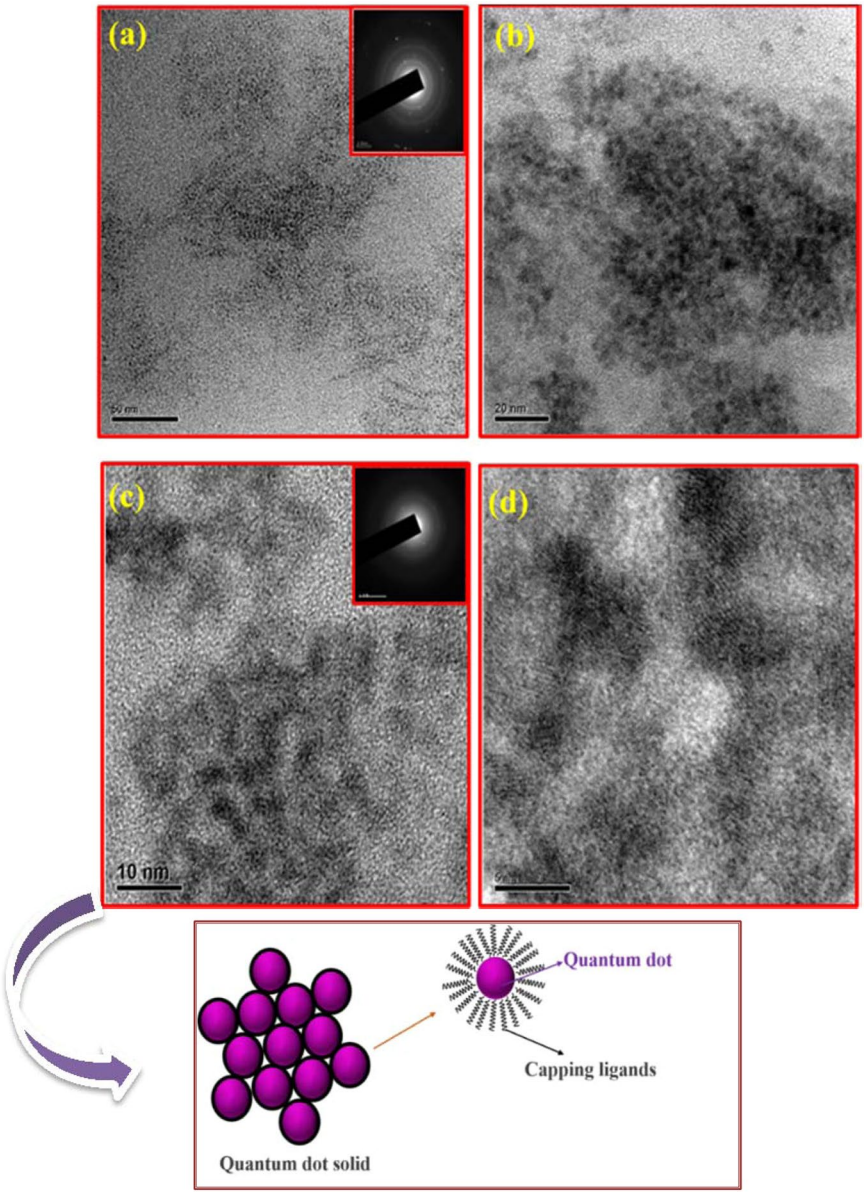

Figure 2. HRTEM analysis of ZnS QDs samples prepared at different reaction time intervals (**a**,**b**) ZnS QD (12 hrs) (**c**,**d**) ZnS QD solid (24 hrs) (inset is SAED pattern of ZnS). Schematic representation of Quantum dot solids (Down).

lattice d-spacing value corresponding to 111 planes of cubic ZnS is found to be 0.22 nm. The lattice fringes visible in the HRTEM confirm the crystalline nature of the ZnS QDs.

In addition, the interaction of ZnS QDs with graphene was investigated by the PL decay lifetime by using TCSPC measurements. Figure 6 shows the PL decay profile of graphene/ZnS QDs samples. The average lifetime values were calculated and presented in Table 2, which indicates the decrease in average lifetime value from 43 ns to 3.7 ns with increasing reaction time from 12 hrs to 48 hrs. On comparing these results to that of bare ZnS QDs sample, it is clear that there must be some electronic interactions between the ZnS QDs and hybridizing graphene, which has resulted in the overall decrease of average lifetime values of hybrid samples[53,54]. The hybridization of ZnS QDs with graphene was further confirmed by the observed shift in D and G Raman bands. The graphene oxide and graphene/ZnS hybrids samples were subjected to Raman analysis and the obtained spectra are shown in Fig. 7(a,b). While two typical peaks of GO can be found at 1357 and 1859 cm^{-1}, corresponding to D and G bands respectively, the hybrid samples exhibit D and G bands at 1353 and 1585 cm^{-1}, respectively. The observed redshift in the Raman bands of hybrid samples, indicated the reduction of graphene oxide and the hybrid formation with ZnS QDs as reported elsewhere[46,59]. In the hybrids samples, the two peaks obtained at D and G bands indicates the sp^2 carbon networks and the relative intensity ratio of the I_D/I_G represents the degree of carbonization. Further, the redshift in the G band position was observed due to the softening of phonons, which indicated the enrichment of electrons in graphene. i.e., the electrons are transferred from ZnS QDs to graphene

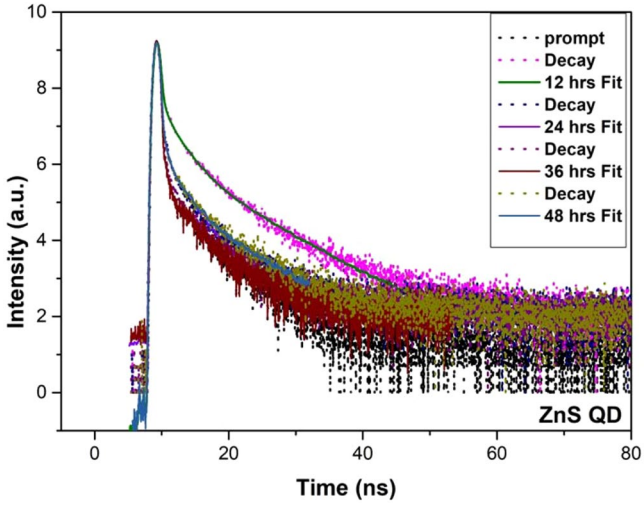

Figure 3. TCSPC lifetime spectra for Pure ZnS QDs prepared at different reaction time intervals (12, 24, 36 and 48 hrs).

Reaction Time	Lifetime [τ_1]	Lifetime [τ_2]	Avg. Lifetime [τ]
ZnS 12 hrs	$\tau_1 = 3.004 \times 10^{-10}$s ($A_1 = 46.72$)	$\tau_2 = 6.44 \times 10^{-8}$s ($A_2 = 53.28$)	$\tau = 64 \times 10^{-9}$s
ZnS 24 hrs	$\tau_1 = 1.4355 \times 10^{-10}$s ($A_1 = 90.70$)	$\tau_2 = 5.730 \times 10^{-9}$s ($A_2 = 9.30$)	$\tau = 4.636 \times 10^{-9}$s
ZnS 36 hrs	$\tau_1 = 1.386 \times 10^{-10}$s ($A_1 = 87.92$)	$\tau_2 = 5.9980 \times 10^{-9}$s ($A_2 = 12.08$)	$\tau = 5.15 \times 10^{-9}$s
ZnS 48 hrs	$\tau_1 = 1.4739 \times 10^{-10}$s ($A_1 = 83.81$)	$\tau_2 = 5.2789 \times 10^{-9}$s ($A_2 = 16.19$)	$\tau = 4.63 \times 10^{-9}$s

Table 1. TCSPC lifetime values for Pure ZnS quantum dot samples at different reaction time intervals.

upon hybrid formation as reported elsewhere[60]. Further, we confirmed the graphene hybrids formation by using FTIR spectra results as shown in Fig. S3.

Photocurrent measurement for ZnS quantum dot solid and its graphene hybrids. The photocurrent characterization of ZnS clusters like quantum dot solid and ZnS QD decorated graphene hybrids were investigated by incorporating them as the active layer in the (FTO/TiO_2/(photosensitizer)/MoO_3/Ag) device structure as shown in Fig. 8; here the photo-sensitizer denotes the as-prepared cluster like ZnS quantum dot solid and ZnS/Graphene hybrid samples (both 24 hrs and 48 hrs samples). The photoresponse curves recorded for the biasing voltages of 0.5 V and 1.0 V are presented in Figs. 9 and 10, respectively. From the photocurrent curves, it is clear that all the samples show higher photocurrent value for the biasing voltage of 1.0 V (compared to the corresponding values measured with 0.5 V biasing voltage). The ZnS QD solid (24 hrs prepared sample), generated the maximum photocurrent values of 1.0 mA and 3.5 mA for the biasing voltages of 0.5 V and 1.0 V as shown in Fig. 9(a). Surprisingly, the ZnS QD solid samples collected at 48 hrs reaction, displayed a sharp rise in the photocurrent to 8.6 mA (for the biasing voltage of 1.0 V), however with a low on/off ratio ($I_{on}/I_{off} = 1.2$) compared with 24 hrs sample, which displayed a better ON-Off ratio of 1.58×10^2 along with a fast response time of <0.05 sec as shown in Fig. 9(a,b). The higher photocurrent value observed in the case of ZnS QD solid samples prepared at 48 hrs reaction time attribute to the QD solid formation as explained in the previously. The observed non-zero dark current could be due to the leakage of charge carriers across the junction in the absence of illumination as reported elsewhere[61,62]. The schematic representation of the electron transfer process is shown in Fig. 9c. Figure 10(a,b) shows the photocurrent response of ZnS QD solid/graphene hybrids 24 hrs and 48 hrs samples, respectively, which indicate the maximum photocurrent values of 1.8 μA and 82 mA, respectively, for a biasing voltage of 1.0 V. The difference in the device performance when compared to 24 hrs ZnS QDs solid/graphene hybrid device can be explained as follows. For the preparation of ZnS QDs solid/graphene hybrid sample, graphene oxide has been used as a precursor. During the hybrid growth process, the GO was reduced as rGO by the hydrazine hydrate, a reducing agent added during the reaction. This reduction of GO further continues and when the reaction time reaches 48 hrs time, the rGO further reduced and etched into graphene quantum dots (GQDs)[43]. We believe that the formation of GQDs contribute the resultant photocurrent and it is because of this reason, the ZnS QD solid/graphene hybrid with 48 hrs prepared device a generated higher photocurrent value of 82 mA. Also, we believe that, in the 48 hrs ZnS QDs solid/graphene hybrids sample, the QD solid formation is nearly complete and therefore it appears like the aggregated QDs.

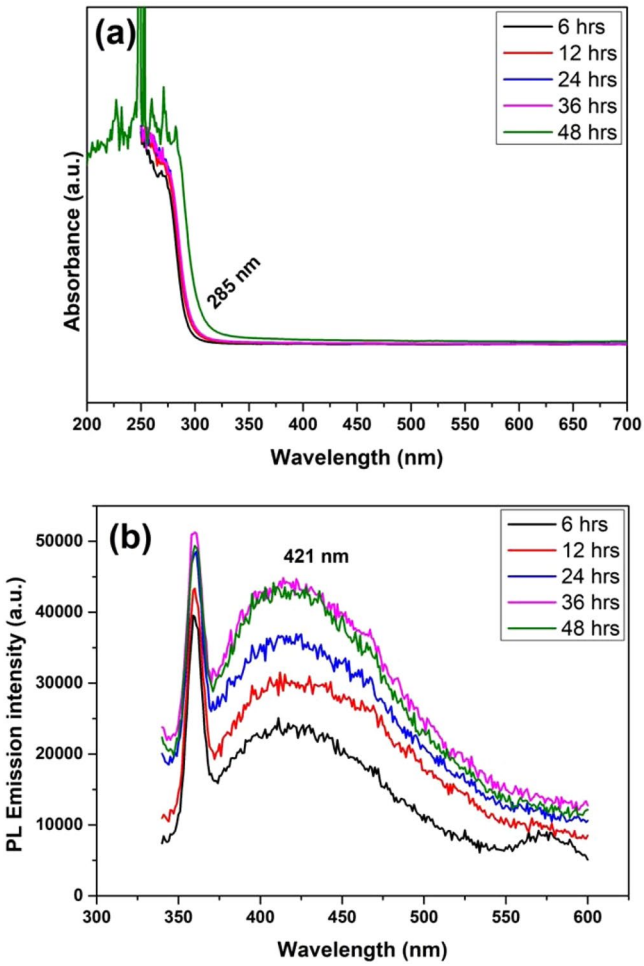

Figure 4. (**a**) UV-vis Absorbance and (**b**) Photoluminescence emission spectra of ZnS QDs with graphene hybrids samples prepared at different reaction time intervals.

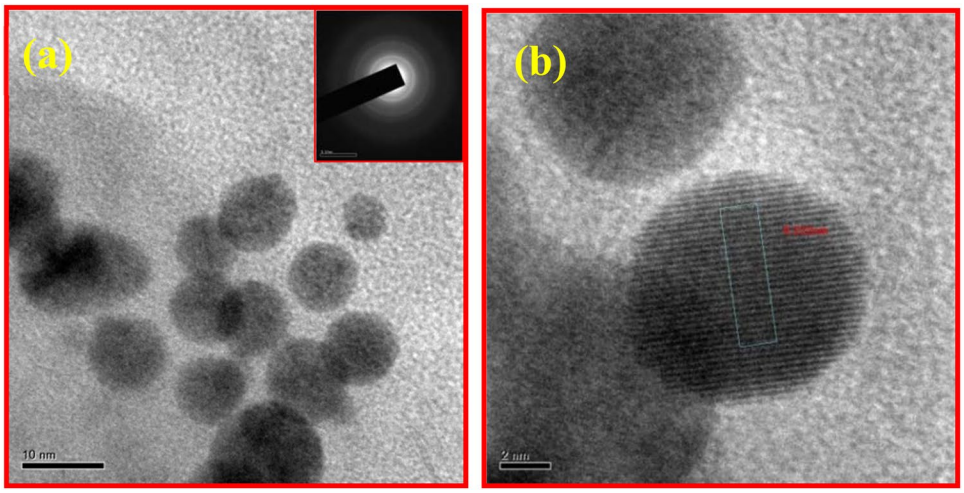

Figure 5. HRTEM images of ZnS QD with graphene hybrids samples: (**a**) Low resolution images of graphene sheets decorated ZnS QDs (24 hrs) and (**b**) High resolution image clearly showing the QD lattice d spacing value of ~0.22 nm with corresponding 111 planes of cubic ZnS.

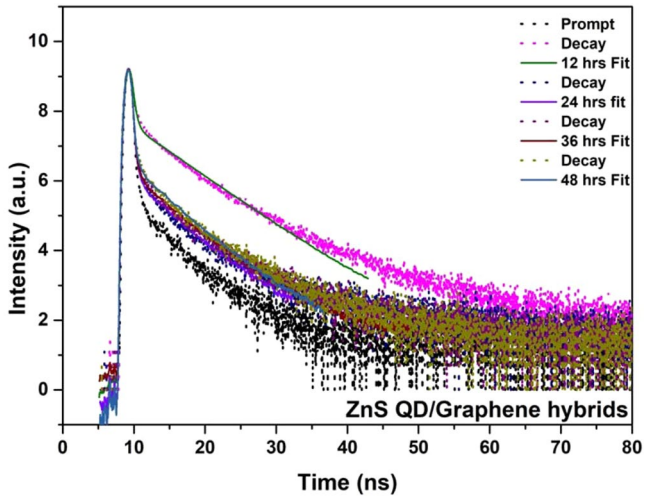

Figure 6. TCSPC lifetime spectra of ZnS/Graphene hybrids prepared at different reaction time intervals (12, 24, 36 and 48 hrs) respectively.

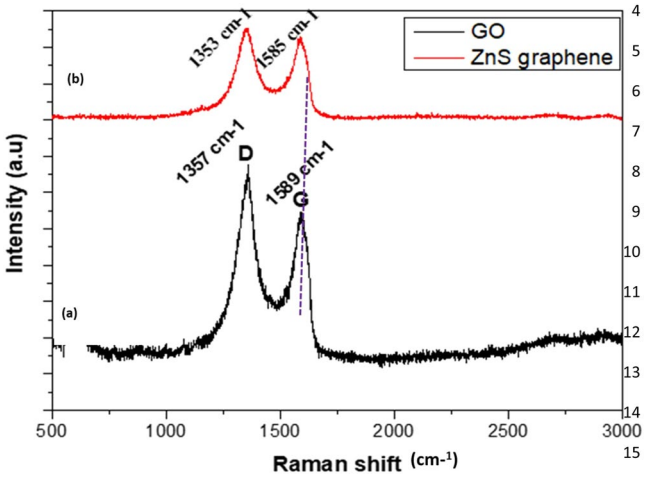

Figure 7. The Raman spectra of (**a**) GO, (**b**) ZnS/Graphene hybrids sample prepared at 24 hrs. Photocurrent measurement for ZnS quantum dot solid and its graphene hybrids.

Reaction Time	Lifetime [τ_1]	Lifetime [τ_2]	Avg. Lifetime [τ]
ZnS/Graphene12 hrs	$\tau_1 = 2.2643 \times 10^{-9}$s ($A_1 = 13.38$)	$\tau_2 = 4.40 \times 10^{-8}$s ($A_2 = 86.62$)	$\tau = 43.67 \times 10^{-9}$s
ZnS/Graphene 24 hrs	$\tau_1 = 1.2490 \times 10^{-10}$s ($A_1 = 91.65$)	$\tau_2 = 2.675 \times 10^{-9}$s ($A_2 = 8.35$)	$\tau = 1.810 \times 10^{-9}$s
ZnS /Graphene 36 hrs	$\tau_1 = 1.9290 \times 10^{-9}$s ($A_1 = 3.20$)	$\tau_2 = 4.218 \times 10^{-8}$s ($A_2 = 3.90$) $\tau_3 = 9.8339 \times 10^{-11}$s ($A_3 = 92.90$)	$\tau = 6.10 \times 10^{-9}$s
ZnS/Graphene 48 hrs	$\tau_1 = 4.801 \times 10^{-9}$s ($A_1 = 8.70$)	$\tau_2 = 1.2813 \times 10^{-10}$s ($A_2 = 91.30$)	$\tau = 3.786 \times 10^{-9}$s

Table 2. TCSPC lifetime values of ZnS QD/Graphene hybrids prepared at different reaction time intervals.

Ultraviolet (UV) sensor device fabrication. The prototype UV sensor devices were fabricated using the as-prepared cluster like ZnS quantum dot solid and ZnS QD solid/Graphene hybrid samples (24 hrs and 48 hrs). The photocurrent device structure was FTO/TiO_2/(active layer)/Ag. The as-prepared ZnS quantum dot solid and ZnS QD/Graphene hybrid samples were coated as the active layer, over the FTO/TiO_2 and finally, the silver electrode was deposited as the top layer using the thermal evaporation technique as shown in Fig. 11. Figure 12 shows the recorded UV photocurrent response curves of the constructed photodetector devices. The photodetector devices constructed using ZnS quantum dot solid 24 hrs and 48 hrs samples displayed the maximum

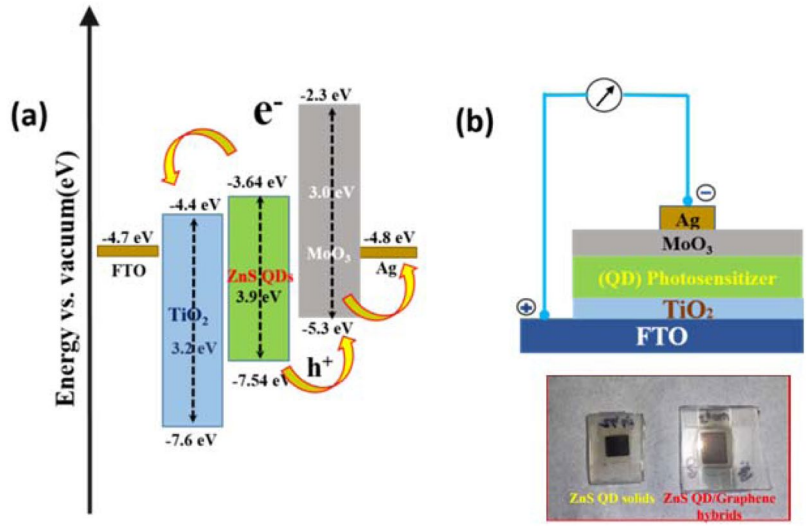

Figure 8. (**a**) Schematic representation of relative energy level position for ZnS QDs solid and (**b**) Photocurrent device structure.

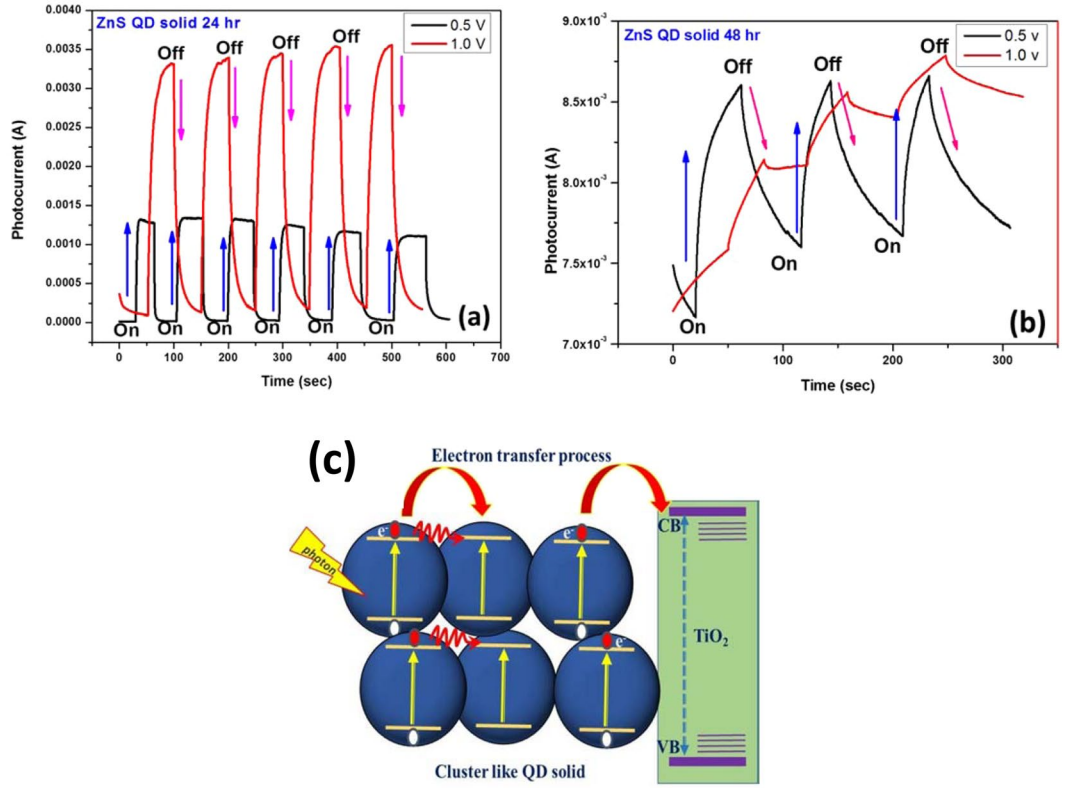

Figure 9. Photocurrent properties for ZnS QD solid prepared at (**a**) 24 hrs, (**b**) 48 hrs, samples recorded at different biasing voltage (0.5 and 1.0)Volt and (**c**) Schematic representation of electron transfer process between the cluster like QD solid and TiO_2 film reducing the electron recombination with increasing electron transfer rate.

photocurrent values of 2.5 μA and 90 nA, respectively, at zero biasing voltage. On the other hand, the devices constructed using ZnS QD solid/Graphene hybrid samples prepared for 24 hrs and 48 hrs, generated the maximum photocurrent values of 0.6 μA and 0.11 mA, respectively (Fig. 12). The higher photocurrent observed in the case of ZnS QD solid/Graphene hybrid is attributed to the incorporation of graphene. The unrelaxed electrons present in the molecular energy levels of graphene add up to the photocurrent as the device ON time progresses. It is because of this reason, the saw tooth wave like pattern is observed for the ZnS QD solid/Graphene hybrid photodetector device. The maximum responsivity of this photodetector device is calculated to be 0.31 (A/W).

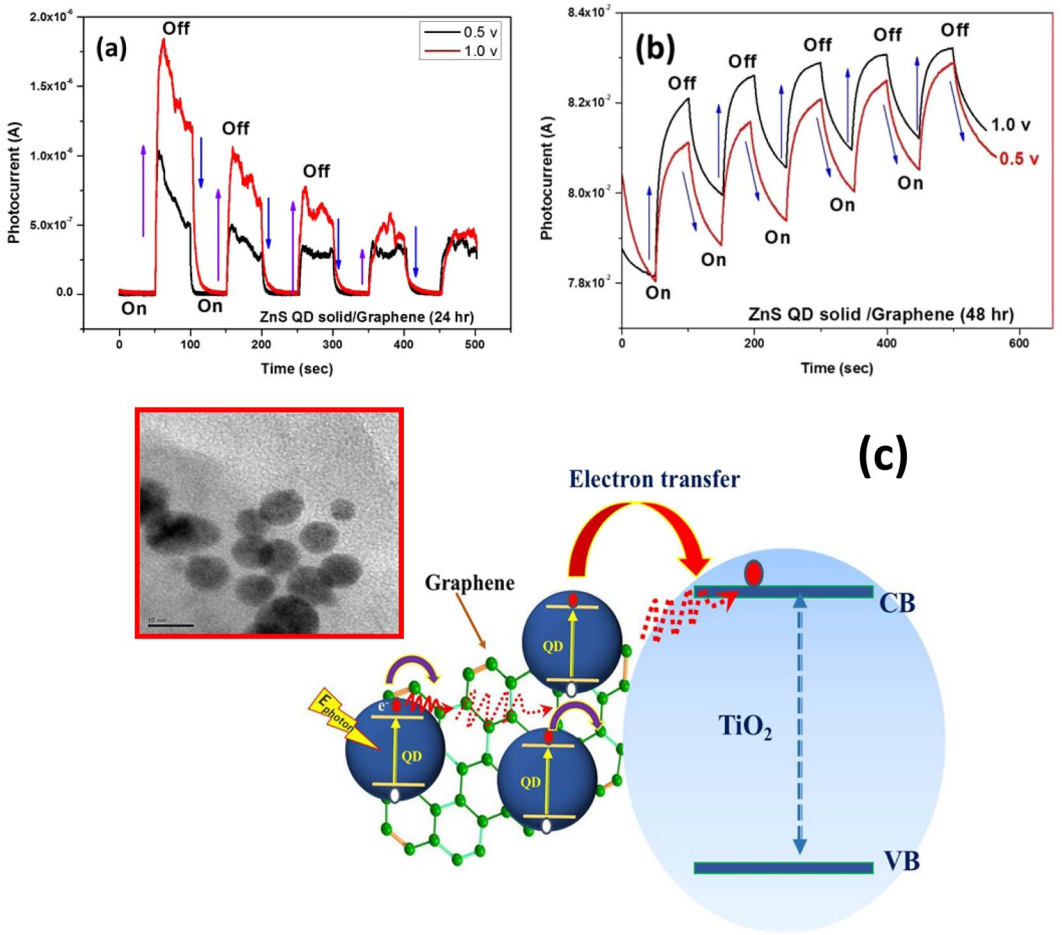

Figure 10. Photocurrent properties for ZnS QD with graphene hybrids (**a**) ZnS QD solid with graphene prepared at 24 hrs (**b**) ZnS QD solid with graphene prepared at 48 hrs, samples recorded at different biasing voltage (0.5 and 1.0)Volt, and (**c**) Schematic representation of electron transfer from QDs/graphene hybrids to TiO_2.

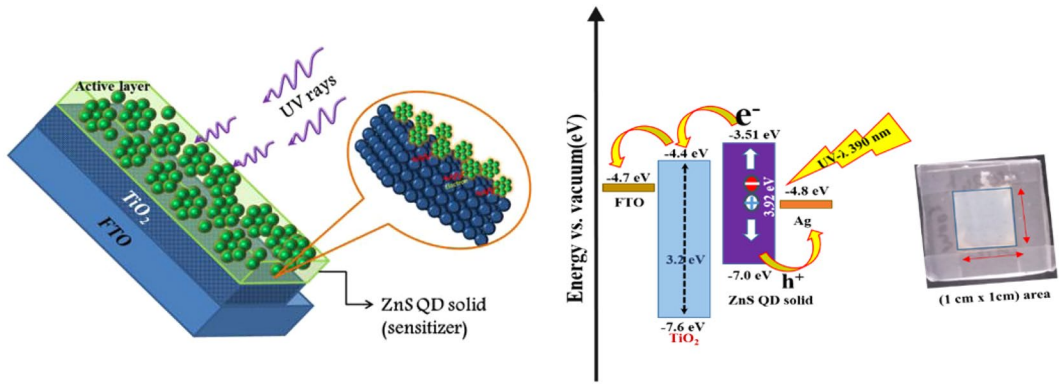

Figure 11. Schematic representation of relative energy level position for ZnS QDs solid (left), UV photo detector based device structure (right).

It is worth noting that, the peak photocurrent of our best device (constructed using ZnS quantum dot solid 24 hrs sample) is much higher compared to the recently reported values[63,64]. Figure 13(a) shows the I-V characteristic curve under Dark and light illumination conditions. The stability curves are included in the Supporting Information (Fig. S4).

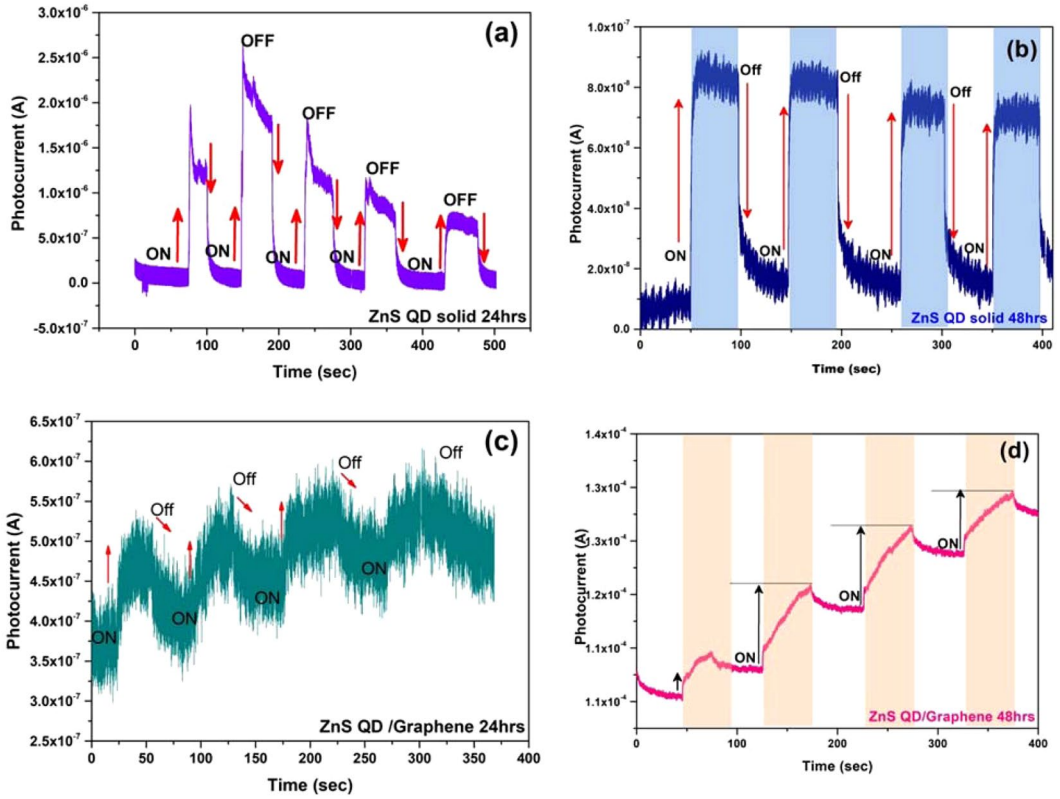

Figure 12. Time-dependent UV response behaviour, measured with turning 390 nm A UV light of 8 µW Cm^2 on and off periodically in ambient condition. (**a**) ZnS QD solid 24 hr, (b) ZnS QD solid 48 hr, (**c**) ZnS QD solid/Graphene hybrid 24 hr and (**d**) ZnS QD solid/Graphene hybrid 48 hr (illumination of UV light ~390 nm).

Discussion

In order to clearly explain the working principle of the UV photodetector device, a simple energy band diagram is schematically presented in Fig. 11. Upon illumination (UV radiation), the device has created a number of photoexcited electrons in the sensitizer (ZnS QD solid), these excited state electrons move from the conduction band of ZnS_{CB} to TiO_{2CB}[65,66]. And then the electrons are transferred to FTO (transparent conducting oxide) at the same time holes were collected from Ag in the favorable energy level position. Generally, quantum dot solid system having high electron mobility[41,42] compared with the normal system, herein, ZnS quantum dots solid system have high electron mobility and delocalized electrons which has resulted in increasing the exciton generation (electron-hole pair) and the corresponding photocurrent as well. The observed photocurrent response under UV light illumination is attributed to the effective collection of photogenerated carriers from the photosensitizer, and the photodetector device shows higher sensitivity towards UV detection. The device exhibited a high magnitude current value under low-intensity UV light source and has the on/off ratio of $I_{UV}/I_{dark} = 413$ at zero biasing voltage along with fast response and recovery time. The best result of our constructed photodetectors exhibited the maximum responsivity of 0.31 (A/W) with a photocurrent value of 2.5 µA at wavelength of $\lambda = 390$ nm.

In summary, the ZnS cluster like quantum dot solid system and ZnS QD decorated Graphene sheet hybrids were successfully prepared and their photophysical and UV photo-sensing properties were investigated in detail. The photophysical characterization of the bare ZnS system tipoff the enhancement in the interdot charge transport upon QD solid formation and provided the evidence for the photoexcited electron transfer from ZnS QDs to graphene in the hybrid system. These results were reflected in the device performances, by showing an enhancement in the photocurrent values of the respective UV sensor devices. Based on the overall device performances, the device constructed using ZnS QD solid 24 hr sample is better suitable for the practical application. Our best UV sensor device exhibited the maximum responsivity of 0.31 (A/W) with a photocurrent value of 2.5 µA at wavelength of $\lambda = 390$ nm.

Methods

Preparation of ZnS quantum dot solid. The ZnS quantum dots solid were prepared by a modified simple chemical route[43,67,68]. $Zn(CH_3CO_2)_2{\cdot}2H_2O$.and Na_2S (purchased from Sigma Aldrich) were dissolved separately in double-distilled water. At first, freshly prepared 5 mmol of Zn (OAc_2) solution was kept in magnetic stirrer. Then varying 50 to 300 µl of 3-mercatopropionic acid (MPA) was added into the above main precursor solution, and the pH of the solution was increased to 9 to 11 by adding NaOH solution. After that, freshly prepared 3 mmole of Na_2S solution was added slowly drop wise into the above solution to get MPA capped ZnS QD. The mixture is loaded in the round bottom flask under an inert atmosphere with the optimized condition. The reaction flask

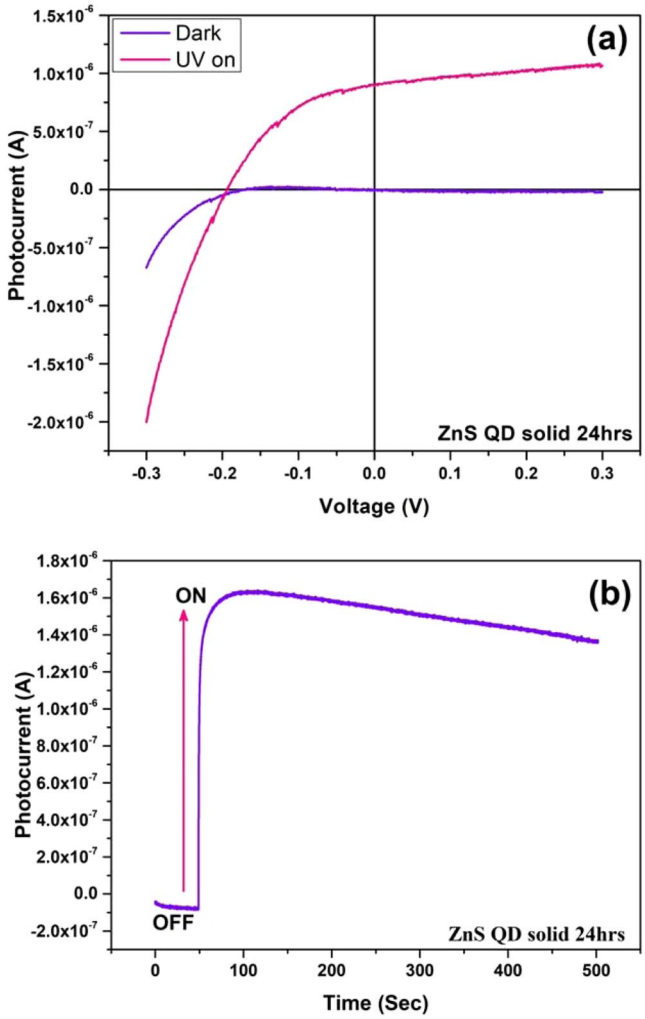

Figure 13. (**a**) I-V Characteristic of a ZnS cluster like QD solid 24 hrs sample based photodetector device under dark condition and UV light (**b**) and Stability curve under continuousUV light (390 nm) illumination.

was maintained at 90 °C with constant stirring, samples were collected at various time intervals (6, 12, 24 and 48 hrs). The white colored colloidal solution was obtained which indicated the formation of ZnS nanocrystal. The sample was washed in (DDW) to remove the unreacted compounds. Further, they were subjected to centrifuge at 5000 rpm for 10 minutes to settle down the particles and then the product was dried at 60 °C under vacuum condition.

Photocurrent device fabrication. The photocurrent device structure planned for the photocurrent measurement was FTO/TiO_2/(photosensitizer)/MoO_3/Ag. Different layers of the device were deposited on the pre-cleaned FTO coated glass slides. TiO_2 coating (active area $1 \times 1\,cm^2$) was obtained by using titania paste (purchased from Sigma Aldrich) on FTO substrate by doctor blade technique[69,70] and the sample was annealed at 450 °C for 6 hrs. The photosensitizer (QD) was deposited by drop cast/spin coating method over the TiO_2 films and dried at ambient temperature for 6 hrs. The MoO_3 (hole transport layer) and Ag top electrodes was deposited (electrode area ($0.5 \times 0.5\,cm^2$) by using thermal evaporation method. The constructed devices were subjected to photocurrent measurements.

Characterization. HRTEM analysis was carried out using a JEOL JEM-2100 at an operating voltage of 200 kV. UV-Vis absorption measurements were carried out by using an Agilent CARY 60 spectrophotometer. PL excitation and emission measurements were carried out using a Horiba Jobin Yvon fluoromax-4 spectrofluorimeter. The PL lifetime measurements were carried out by using an IBH time-correlated single photon counting (TCSPC) system. The samples were characterized by RAMAN measurements using a Horiba LABRAM HR excited by a 514-nm laser. Photocurrent measurement was carried by using a 300 Watt xenon lamp as an illumination source and a source measuring unit (Agilent B2912A) was used to record the photocurrent values. The photodetector measurements were carried using a UV light source illumination with $\lambda = 390$ nm and $8\,\mu W\,cm^2$ power.

Received: 15 July 2019; Accepted: 19 November 2019;
Published online: 10 December 2019

References

1. Khan, F., Khan, W. & Kim, S.-D. High-Performance Ultraviolet Light Detection Using Nano-Scale-Fin Isolation AlGaN/GaN Heterostructures with ZnO Nanorods. *Nanomaterials (Basel)* **9**, 440, https://doi.org/10.3390/nano9030440 (2019).
2. Guo, Y., Li, Y., Zhang, Q. & Wang, H. Self-powered multifunctional UV and IR photodetector as an artificial electronic eye. *Journal of Materials Chemistry C* **5**, 1436–1442, https://doi.org/10.1039/c6tc04771h (2017).
3. Tian, B. *et al*. Coaxial silicon nanowires as solar cells and nanoelectronic power sources. *Nature* **449**, 885, https://doi.org/10.1038/nature06181, https://www.nature.com/articles/nature06181#supplementary-information (2007).
4. Monroy, E., Omn, S. F. & Calle, F. Wide-bandgap semiconductor ultraviolet photodetectors. *Semiconductor Science and Technology* **18**, R33–R51, https://doi.org/10.1088/0268-1242/18/4/201 (2003).
5. Shen, T. *et al*. Surface Engineering of Quantum Dots for Remarkably High Detectivity Photodetectors. *The Journal of Physical Chemistry Letters* **9**, 3285–3294, https://doi.org/10.1021/acs.jpclett.8b01255 (2018).
6. Wan, X. *et al*. A self-powered high-performance graphene/silicon ultraviolet photodetector with ultra-shallow junction: breaking the limit of silicon? *npj 2D Materials and Applications* **1**, 4, https://doi.org/10.1038/s41699-017-0008-4 (2017).
7. Nakagomi, S., Momo, T., Takahashi, S. & Kokubun, Y. Deep ultraviolet photodiodes based on β-Ga2O3/SiC heterojunction. *Applied Physics Letters* **103**, 072105, https://doi.org/10.1063/1.4818620 (2013).
8. Zheng, X. J. *et al*. A photoconductive semiconductor switch based on an individual ZnS nanobelt. *Scripta Materialia* **62**, 520–523, https://doi.org/10.1016/j.scriptamat.2009.12.031 (2010).
9. Moun, M., Kumar, M., Garg, M., Pathak, R. & Singh, R. Understanding of MoS2/GaN Heterojunction Diode and its Photodetection Properties. *Scientific Reports* **8**, 11799, https://doi.org/10.1038/s41598-018-30237-8 (2018).
10. Sun, X. *et al*. High spectral response of self-driven GaN-based detectors by controlling the contact barrier height. *Scientific Reports* **5**, 16819, https://doi.org/10.1038/srep16819 (2015).
11. Jia, R., Zhao, D., Gao, N. & Liu, D. Polarization Enhanced Charge Transfer: Dual-Band GaN-Based Plasmonic Photodetector. *Scientific Reports* **7**, 40483, https://doi.org/10.1038/srep40483 (2017).
12. Bai, S. *et al*. High-Performance Integrated ZnO Nanowire UV Sensors on Rigid and Flexible Substrates. *Advanced Functional Materials* **21**, 4464–4469, https://doi.org/10.1002/adfm.201101319 (2011).
13. Yang, S., Gong, J. & Deng, Y. Opposite photocurrent response to ultraviolet and visible light. *Journal of Materials Chemistry* **22**, 24522–24525, https://doi.org/10.1039/c2jm34545e (2012).
14. Huang, X. *et al*. Ultraviolet photodetectors with high photosensitivity based on type-II ZnS/SnO2 core/shell heterostructured ribbons. *Nanoscale* **7**, 5311–5319, https://doi.org/10.1039/c5nr00150a (2015).
15. Qian, L. X. *et al*. β-Ga2O3 solar-blind deep-ultraviolet photodetector based on a four-terminal structure with or without Zener diodes. *AIP Advances* **6**, 045009, https://doi.org/10.1063/1.4947137 (2016).
16. Takayoshi, O., Takeya, O. & Shizuo, F. Ga 2 O 3 Thin Film Growth on c -Plane Sapphire Substrates by Molecular Beam Epitaxy for Deep-Ultraviolet Photodetectors. *Japanese Journal of Applied Physics* **46**, 7217 (2007).
17. Mueller, T., Xia, F. & Avouris, P. Graphene photodetectors for high-speed optical communications. *Nature Photonics* **4**, 297, https://doi.org/10.1038/nphoton.2010.40, https://www.nature.com/articles/nphoton.2010.40#supplementary-information (2010).
18. Alivisatos, A. P. Semiconductor Clusters, Nanocrystals, and Quantum Dots. *Science* **271**, 933–937, https://doi.org/10.1126/science.271.5251.933 (1996).
19. Tian, P., Tang, L., Teng, K. S. & Lau, S. P. Graphene quantum dots from chemistry to applications. *Materials Today. Chemistry* **10**, 221–258, https://doi.org/10.1016/j.mtchem.2018.09.007 (2018).
20. Bera, A. & Basak, D. Role of defects in the anomalous photoconductivity in ZnO nanowires. *Applied Physics Letters* **94**, 163119, https://doi.org/10.1063/1.3123167 (2009).
21. Razeghi, M. & Rogalski, A. Semiconductor ultraviolet detectors. *Journal of Applied Physics* **79**, 7433–7473, https://doi.org/10.1063/1.362677 (1996).
22. Lhuillier, E. *et al*. Infrared Photodetection Based on Colloidal Quantum-Dot Films with High Mobility and Optical Absorption up to THz. *Nano Letters* **16**, 1282–1286, https://doi.org/10.1021/acs.nanolett.5b04616 (2016).
23. Fang, X. *et al*. Single-Crystalline ZnS Nanobelts as Ultraviolet-Light Sensors. *Advanced Materials* **21**, 2034–2039, https://doi.org/10.1002/adma.200802441 (2009).
24. Ganatra, R. & Zhang, Q. Few-Layer MoS2: A Promising Layered Semiconductor. *ACS Nano* **8**, 4074–4099, https://doi.org/10.1021/nn405938z (2014).
25. Peng, L., Hu, L. & Fang, X. Low-Dimensional Nanostructure Ultraviolet Photodetectors. *Advanced Materials* **25**, 5321–5328, https://doi.org/10.1002/adma.201301802 (2013).
26. Zhai, T. *et al*. Recent Developments in One-Dimensional Inorganic Nanostructures for Photodetectors. *Advanced Functional Materials* **20**, 4233–4248, https://doi.org/10.1002/adfm.201001259 (2010).
27. An, Q., Meng, X., Xiong, K. & Qiu, Y. Self-powered ZnS Nanotubes/Ag Nanowires MSM UV Photodetector with High On/Off Ratio and Fast Response Speed. *Scientific Reports* **7**, 4885, https://doi.org/10.1038/s41598-017-05176-5 (2017).
28. Kim, Y., Kim, S. J., Cho, S.-P., Hong, B. H. & Jang, D.-J. High-performance ultraviolet photodetectors based on solution-grown ZnS nanobelts sandwiched between graphene layers. *Scientific Reports* **5**, 12345, https://doi.org/10.1038/srep12345, https://www.nature.com/articles/srep12345#supplementary-information (2015).
29. Huang, F. *et al*. High- and Reproducible-Performance Graphene/II-VI Semiconductor Film Hybrid Photodetectors. *Scientific Reports* **6**, 28943, https://doi.org/10.1038/srep28943, https://www.nature.com/articles/srep28943#supplementary-information (2016).
30. Sun, Y.-L. *et al*. Hybrid graphene/cadmium-free ZnSe/ZnS quantum dots phototransistors for UV detection. *Scientific Reports* **8**, 5107, https://doi.org/10.1038/s41598-018-23507-y (2018).
31. Hu, L. *et al*. An Optimized Ultraviolet-A Light Photodetector with Wide-Range Photoresponse Based on ZnS/ZnO Biaxial Nanobelt. *Advanced Materials* **24**, 2305–2309, https://doi.org/10.1002/adma.201200512 (2012).
32. Yu, Y. *et al*. High-gain visible-blind UV photodetectors based on chlorine-doped n-type ZnS nanoribbons with tunable optoelectronic properties. *Journal of Materials Chemistry* **21**, 12632–12638, https://doi.org/10.1039/c1jm11408e (2011).
33. Jiang, P. *et al*. Aluminium-doped n-type ZnS nanowires as high-performance UV and humidity sensors. *Journal of Materials Chemistry* **22**, 6856–6861, https://doi.org/10.1039/c2jm15365c (2012).
34. Chen, H., Liu, H., Zhang, Z., Hu, K. & Fang, X. Nanostructured Photodetectors: From Ultraviolet to Terahertz. *Advanced Materials* **28**, 403–433, https://doi.org/10.1002/adma.201503534 (2016).
35. Wang, X., Tian, W., Liao, M., Bando, Y. & Golberg, D. Recent advances in solution-processed inorganic nanofilm photodetectors. *Chemical Society Reviews* **43**, 1400–1422, https://doi.org/10.1039/c3cs60348b (2014).
36. Han, Y. D. *et al*. Quantum dot and π-conjugated molecule hybrids: nanoscale luminescence and application to photoresponsive molecular electronics. *Npg Asia Materials* **6**, e103, https://doi.org/10.1038/am.2014.28, https://www.nature.com/articles/am201428#supplementary-information (2014).
37. Zeng, B. *et al*. Characterization of the Ligand Capping of Hydrophobic CdSe–ZnS Quantum Dots Using NMR Spectroscopy. *Chemistry of Materials* **30**, 225–238, https://doi.org/10.1021/acs.chemmater.7b04204 (2018).

38. Wilker, M. B. *et al*. Role of Surface-Capping Ligands in Photoexcited Electron Transfer between CdS Nanorods and [FeFe] Hydrogenase and the Subsequent H2 Generation. *The Journal of Physical Chemistry C* **122**, 741–750, https://doi.org/10.1021/acs.jpcc.7b07229 (2018).
39. Green, M. The nature of quantum dot capping ligands. *Journal of Materials Chemistry* **20**, 5797–5809, https://doi.org/10.1039/c0jm00007h (2010).
40. Li, T.-L., Lee, Y.-L. & Teng, H. High-performance quantum dot-sensitized solar cells based on sensitization with CuInS2 quantum dots/CdS heterostructure. *Energy & Environmental Science* **5**, 5315–5324, https://doi.org/10.1039/c1ee02253a (2012).
41. Kagan, C. R., Murray, C. B., Nirmal, M. & Bawendi, M. G. Electronic Energy Transfer in CdSe Quantum Dot Solids. *Physical Review Letters* **76**, 1517–1520, https://doi.org/10.1103/PhysRevLett.76.1517 (1996).
42. Ihly, R., Tolentino, J., Liu, Y., Gibbs, M. & Law, M. The Photothermal Stability of PbS Quantum Dot Solids. *ACS Nano* **5**, 8175–8186, https://doi.org/10.1021/nn2033117 (2011).
43. Premkumar, S., Nataraj, D., Bharathi, G., Khyzhun, O. Y. & Thangadurai, T. D. Interfacial Chemistry-Modified QD-Coupled CdTe Solid Nanowire and Its Hybrid with Graphene Quantum Dots for Enhanced Photocurrent Properties. *ChemistrySelect* **2**, 10771–10781, https://doi.org/10.1002/slct.201702352 (2017).
44. Bharathi, G. *et al*. Graphene Quantum Dot Solid Sheets: Strong blue-light-emitting & photocurrent-producing band-gap-opened nanostructures. *Scientific Reports* **7**, 10850, https://doi.org/10.1038/s41598-017-10534-4 (2017).
45. Cao, J. *et al*. One-step hydrothermal synthesis of shape-controlled ZnS–graphene oxide nanocomposites. *Journal of Materials Science: Materials in Electronics* **26**, 646–650, https://doi.org/10.1007/s10854-014-2444-7 (2015).
46. Pan, S. & Liu, X. ZnS–Graphene nanocomposite: Synthesis, characterization and optical properties. *Journal of Solid State Chemistry* **191**, 51–56, https://doi.org/10.1016/j.jssc.2012.02.048 (2012).
47. Zhang, Q. *et al*. Polar-surface-driven growth of ZnS microsprings with novel optoelectronic properties. *Npg Asia Materials* **7**, e213, https://doi.org/10.1038/am.2015.100, https://www.nature.com/articles/am2015100#supplementary-information (2015).
48. Lee, J. K. *et al*. Ultraintense UV emission from ZnO-sheathed ZnS nanorods. *Scientific Reports* **7**, 13034, https://doi.org/10.1038/s41598-017-13556-0 (2017).
49. Geim, A. K. & Novoselov, K. S. The rise of graphene. *Nat Mater* **6**, 183–191 (2007).
50. Kim, T. Y., Park, C.-H. & Marzari, N. The Electronic Thermal Conductivity of Graphene. *Nano Letters* **16**, 2439–2443, https://doi.org/10.1021/acs.nanolett.5b05288 (2016).
51. Jang, S., Hwang, E., Lee, Y., Lee, S. & Cho, J. H. Multifunctional Graphene Optoelectronic Devices Capable of Detecting and Storing Photonic Signals. *Nano Letters* **15**, 2542–2547, https://doi.org/10.1021/acs.nanolett.5b00105 (2015).
52. Lightcap, I. V. & Kamat, P. V. Fortification of CdSe Quantum Dots with Graphene Oxide. Excited State Interactions and Light Energy Conversion. *Journal of the American Chemical Society* **134**, 7109–7116, https://doi.org/10.1021/ja3012929 (2012).
53. Markad, G. B., Battu, S., Kapoor, S. & Haram, S. K. Interaction between Quantum Dots of CdTe and Reduced Graphene Oxide: Investigation through Cyclic Voltammetry and Spectroscopy. *The Journal of Physical Chemistry C* **117**, 20944–20950, https://doi.org/10.1021/jp406679s (2013).
54. Kundu, S., Sadhu, S., Bera, R., Paramanik, B. & Patra, A. Fluorescence Dynamics and Stochastic Model for Electronic Interaction of Graphene Oxide with CdTe QD in Graphene Oxide-CdTe QD Composite. *The Journal of Physical Chemistry C* **117**, 23987–23995, https://doi.org/10.1021/jp405712p (2013).
55. Yu, P. *et al*. Efficient electron transfer in carbon nanodot-graphene oxide nanocomposites. *Journal of Materials Chemistry C* **2**, 2894–2901, https://doi.org/10.1039/c3tc32395a (2014).
56. Liu, J., Durstock, M. & Dai, L. Graphene oxide derivatives as hole- and electron-extraction layers for high-performance polymer solar cells. *Energy & Environmental Science* **7**, 1297–1306, https://doi.org/10.1039/c3ee42963f (2014).
57. Kaniyankandy, S., Rawalekar, S. & Ghosh, H. N. Ultrafast Charge Transfer Dynamics in Photoexcited CdTe Quantum Dot Decorated on Graphene. *The Journal of Physical Chemistry C* **116**, 16271–16275, https://doi.org/10.1021/jp303712y (2012).
58. Krzyszkowska, E., Walkowiak-Kulikowska, J., Stienen, S. & Wojcik, A. Thionine–graphene oxide covalent hybrid and its interaction with light. *Physical Chemistry Chemical Physics* **19**, 14412–14423, https://doi.org/10.1039/c7cp01267e (2017).
59. Zhang, Y., Zhang, N., Tang, Z.-R. & Xu, Y.-J. Graphene Transforms Wide Band Gap ZnS to a Visible Light Photocatalyst. The New Role of Graphene as a Macromolecular Photosensitizer. *ACS Nano* **6**, 9777–9789, https://doi.org/10.1021/nn304154s (2012).
60. Zhang, Z., Fang, C., Bing, X. & Lei, Y. Graphene Quantum Dots-ZnS Nanocomposites with Improved Photoelectric Performances. *Materials (Basel)* **11**, 512, https://doi.org/10.3390/ma11040512 (2018).
61. Liu, H. C., Steele, A. G., Wasilewski, Z. R. & Buchanan, M. *Dark current mechanism and the cause of the current-voltage asymmetry in quantum-well intersubband photodetectors*. Vol. 1985 PCM (SPIE, 1993).
62. Sverdlov, B. N., Botchkarev, A. E., Teraguchi, N., Salvador, A. A. & Morkoc, H. Reduction of dark current in photodiodes by the use of a resonant cavity. *Electronics Letters* **29**, 1019–1021, https://doi.org/10.1049/el:19930680 (1993).
63. Kumar, V., Rawal, I., Kumar, V. & Goyal, P. K. Efficient UV photodetectors based on Ni-doped ZnS nanoparticles prepared by facial chemical reduction method. *Physica B: Condensed Matter* **575**, 411690, https://doi.org/10.1016/j.physb.2019.411690 (2019).
64. Xia, Y. *et al*. Solution-processed solar-blind deep ultraviolet photodetectors based on strongly quantum confined ZnS quantum dots. *Journal of Materials Chemistry C* **6**, 11266–11271, https://doi.org/10.1039/c8tc03977a (2018).
65. Wang, H. & Kim, D. H. Perovskite-based photodetectors: materials and devices. *Chemical Society Reviews* **46**, 5204–5236, https://doi.org/10.1039/c6cs00896h (2017).
66. Ding, C. *et al*. Understanding charge transfer and recombination by interface engineering for improving the efficiency of PbS quantum dot solar cells. *Nanoscale Horizons* **3**, 417–429, https://doi.org/10.1039/c8nh00030a (2018).
67. Zhang, Z. H., Chin, W. S. & Vittal, J. J. Water-Soluble CdS Quantum Dots Prepared from a Refluxing Single Precursor in Aqueous Solution. *The Journal of Physical Chemistry B* **108**, 18569–18574, https://doi.org/10.1021/jp0470849 (2004).
68. Mandal, A., Dandapat, A. & De, G. Magic sized ZnS quantum dots as a highly sensitive and selective fluorescence sensor probe for Ag+ ions. *Analyst* **137**, 765–772, https://doi.org/10.1039/c1an15653e (2012).
69. Bernacka-Wojcik, I. *et al*. Inkjet printed and "doctor blade" TiO2 photodetectors for DNA biosensors. *Biosensors and Bioelectronics* **25**, 1229–1234, https://doi.org/10.1016/j.bios.2009.09.027 (2010).
70. Kontos, A. I. *et al*. Nanostructured TiO2 films for DSSCS prepared by combining doctor-blade and sol–gel techniques. *Journal of Materials Processing Technology* **196**, 243–248, https://doi.org/10.1016/j.jmatprotec.2007.05.051 (2008).

Acknowledgements

Author GB acknowledges the University Grants Commission, Govt. of India, for providing BSR fellowship, (G2/5357/UGC-BSR-Research Fellowship/2013). DN acknowledges Department of Science and Technology, Govt. of India, for the research funding under DST-SERI scheme (DST/TM/SERI/FR/232/G). DN also acknowledges (UGC-CPEPA) Centre for Advanced Studies in Physics for the development of Solar Energy Materials and Devices (2–8/2016(NS/PE)). DN acknowledges RUSA Program Phase I (Component-8) Research and Innovation, India. SR acknowledges the University Grants Commission, Govt. of India, for providing BSR fellowship, (G2/30620/798UGC-BSR-Research Fellowship/2015).

Author contributions

Authors S.P. and D.N. conceived the idea. S.P. prepared the samples. S.P. G.B and S.R. performed the structural and optical characterization and collected the data. S.R. and S.P contributed to the photocurrent device construction and measurements. T.D.T contributed to the FTIR characterization support. S.P. and D.N. wrote the manuscript and all other authors took part in their respective data analysis.

Competing interests

The authors declare no competing interests.

Additional information

Supplementary information is available for this paper at https://doi.org/10.1038/s41598-019-55097-8.

Correspondence and requests for materials should be addressed to S.P. or D.N.

Reprints and permissions information is available at www.nature.com/reprints.

Publisher's note Springer Nature remains neutral with regard to jurisdictional claims in published maps and institutional affiliations.